Fabrication of high-flux defect-free hollow fiber membranes derived from a phenolphthalein-based copolyimide for gas separation

Fabrication of high-flux defect-free hollow fiber membranes derived from a phenolphthalein-based copolyimide for gas separation

Bo Chen[a], Guoke Zhao[b], Cher Hon Lau[c], Fuwei Wang[a], Shuxin Fan[a], Chuang Niu[a], Zhongzheng Ren[a], Gongqing Tang[b], Peiyong Qin[d,*], Yiqun Liu[b,*], Pei Li[a,*]

a College of Materials Science and Engineering, Beijing University of Chemical Technology, Beijing, 100029, China

b SINOPEC Beijing Research Institute of Chemical Industry, Beijing 100013, China

c Institute for Materials and Processes School of Engineering, University of Edinburgh

d College of Life Science and Technology, Beijing University of Chemical Technology, Beijing, 100029, China

*Corresponding authors.

E-mail addresses: liuyq.bjhy@sinopec.com (Y. Liu), qinpeiyong@tsinghua.org.cn (P. Qin), lipei@mail.buct.edu.cn (P. Li).

Abstract:

In the realm of gas purifications, hollow fiber membranes have gained significant prominence due to their unique advantages. However, achieving defect-free membranes poses a considerable challenge. In this study, we addressed this challenge with a novel copolymer, 6FDA-DAM:DAP(2:1), comprising 4,4'-(hexafluoroisopropylidene) diphthalic anhydride (6FDA), 2,4.6-Trimethy-m-phenylenediamine (DAM), and a phenolphthalein-derived diamine of 3,3'-diaminophenolphthalein (DAP). We found that defect-free hollow fiber membranes could be prepared when 20 wt.% or more ethanol was added in the polymer dope solution, but this led to the formation of oval hollow fibers that would be flattened under high pressure. We solved this limitation by lowering ethanol content to 15 wt. %, adding 2 wt. % $LiNO_3$, and increasing the air-gap distance. These measures reduced the difference in phase inversion rates between the surface region and the bulk phase of the nascent hollow fiber. The CO_2 permeance of this defect-free hollow fiber membrane reached 282 GPU with a CO_2/CH_4 selectivity of 50.2. Highly permeable defective hollow fiber membranes were also developed using a polymer dope without $LiNO_3$ and a low THF content of 5 wt.%. After coated by silicone rubber, the CO_2 permeance of the membrane reached 554 GPU with a CO_2/CH_4 selectivity of 45.0. In mixed gas tests, the two membranes exhibited O_2 permeances of approximately 43.3 and 75.3 GPU, with O_2/N_2 selectivities of 5.5 and 5.4, respectively. Their CO_2 permeances were 281 and 465 GPU, with CO_2/CH_4 selectivities of 45 and 41, CO_2/N_2 selectivities of 35.7 and 33.3, respectively. These separation performances out-performed state-of-art

polymeric hollow fiber membranes and demonstrated great potential for gas separation applications such as natural gas sweetening, flue gas treatment, and air separation.

Keywords:

Hollow fiber, Defect-free, 6FDA-DAM:DAP copolyimide, Gas Separation

1. Introduction:

The increasing global demand for clean and sustainable energy sources has accentuated the significance of efficient natural gas separation technologies[1, 2]. Natural gas, as a significant energy resource, is often mixed with carbon dioxide, which not only corrodes pipelines but also reduces the heating value of natural gas. Flue gases, produced by industry and power plants, contain CO_2 and N_2. It is of great interest to capture and utilize CO_2 from flue gas for environmental compliance[3]. Similarly, air separation is also important to produce high purity O_2 and N_2 for medical and industrial applications[4]. Therefore, there is a great demand for gas separation technologies. Conventional separation methods, such as distillation and absorption, are energy-intensive and economically demanding[5]. Membrane technology, especially polymeric membranes have emerged as promising candidates for gas separation due to its higher efficiency, low cost, environmental friendliness, minimal footprint, and capability for continuous operation[6-9]. Asymmetric hollow fiber membrane is the main membrane configuration used in industry.

Hollow fiber membranes offer superior fluid flow, efficient separation, and versatile fabrication compared to other membrane types. Their hollow structure provides increased surface area for enhanced transport, making them ideal for various gas separation applications. Fabrication of asymmetric hollow fibers with thin, defect-free skin layer remains a challenge due to the precise control required over dope composition and spinning process variables. The skin layer of hollow fibers often exhibits defects, leading to a loss of gas selectivity. Post-treatment can restore the gas

separation performance of the membrane[10]. However, this enhanced selectivity comes at the expense of reduced membrane flux and additional costs and it tends to cause instability under aggressive feeds at high pressures and with high concentrations of CO_2[11]. Therefore, achieving defect-free hollow fibers without the need for post-treatment, under carefully optimized spinning conditions, is a highly favorable choice for industrial gas separation applications. Examples of such hollow fiber membranes include those fabricated from polysulfone, cellulose acetate[12-14], 6FDA-based polyimides[15-18], of which their separation properties are listed in Table S4 and S5 in the Supporting Information.

Of particular interest are 6FDA-based polyimides, as these materials offer high rigidity, and tunable transport properties[19]. Gas transportation in these polymers can be tailored by judicious choice of diamines. For example, the 6FDA-DAM polyimide possesses a high CO_2 permeability of 817 Barrer but a low CO_2/CH_4 selectivity of 17.6[16]. In our prior research, we synthesized a phenolphthalein-derived diamine (DAP) through the nitration and reduction of phenolphthalein[20]. This DAP possesses a crosslinkable internal ester group that enhances CO_2/CH_4 selectivity but suppresses CO_2 permeability. The 6FDA-DAP polyimide has a CO_2 permeability of 20.2 Barrer with a CO_2/CH_4 selectivity of 34.2[21]. Here we hypothesize that the lower gas selectivity of 6FDA-DAM and the limited gas permeability of 6FDA-DAP can be overcomed by combining these two moieties into a copolymer, 6FDA-DAM-DAP.

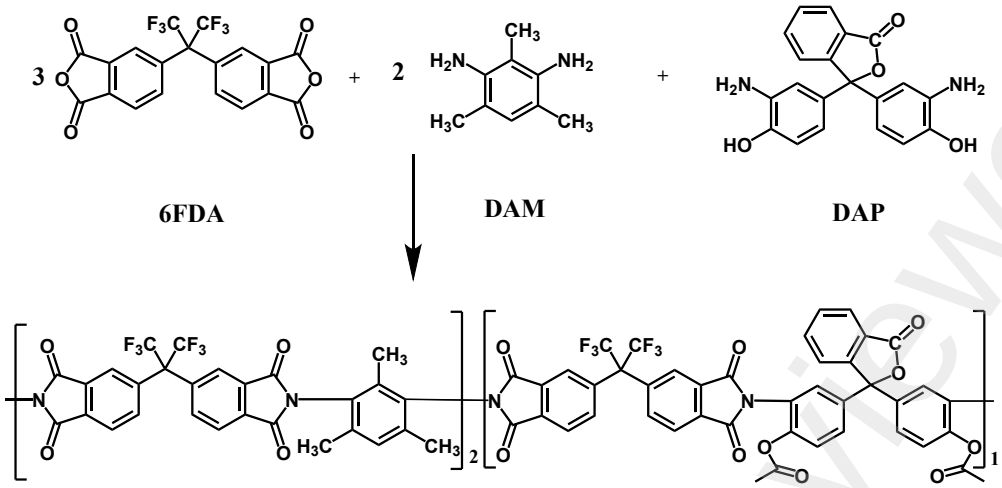

Scheme 1. Reaction scheme for synthesizing a copolyimide of 6FDA-DAM:DAP(2:1).

To validate this hypothesis, here we synthesized a 6FDA-DAM:DAP (2:1) copolymer by co-polymerizing 6FDA and DAM with the self-prepared diamine monomer (DAP) using the chemistry outlined in Scheme 1. We used the dry wet spinning technique to fabricate hollow fiber membranes from this novel copolymer. By exploring the solubility, viscosity, and binodal of the new polymer, we optimized polymer dope concentrations. Here we report that defect-free hollow fiber membranes from 6FDA-DAM-DAP (2:1) could be prepared when the dope solution contained a ethanol concentration of up to 20 wt.%. However, this led to the formation of oval-shaped hollow fibers that flattened under a high pressure of 30 bar, which is typical of operating conditions in industry. We resolved this limitation by lowering ethanol content, adding $LiNO_3$, and increasing the air-gap distance. These measures reduced the difference in the phase inversion rate between the surface region and the bulk phase of the nascent hollow fiber. By overcoming these limitations typically associated with spinning hollow fiber membranes from 6FDA-based polyimides, our approach can

potentially provide a pathway towards commercializing such high performance membranes to improve efficiency of gas separation applications.

2. Experimental

2.1. Materials

4,4'-(hexafluoroisopropylidene) diphthalic anhydride (6FDA) with a purity of 98% was bought from Alfachem. 3,3'-diaminophenolphthalein (DAP) was synthesized using a method introduced by Du. *et. al*[20]. 2,4.6-Trimethy-m-phenylenediamine (DAM) was purchased from Adamas-beta (China). Acetic anhydride was bought from National Pharmaceutical Group (China). Pyridine was obtained from FuGuang Technology (Tianjin, China). 1-Methyl-2-pyrrolidinone (NMP) was purchased from Tianjin Fu Chen Chemical Reagents Factory (Tianjin, China). Ethanol was bought from Beijing Chemical Works (Beijing, China). 6FDA were purified by vacuum sublimation. Polydimethylsiloxane (PDMS, sylgard 184) was obtained from Dow Chemicals.

2.2. Synthesis of copolyimide

The chemical structure of 6FDA-DAM:DAP(2:1) copolyimide is shown in Scheme 1. The copolyimide was synthesized using a two-step chemical imidization method[22]. Firstly, DAM (43.26 g) and DAP (50.16 g) at a molar ratio of 2:1 were dissolved in 450 g NMP in a N_2 environment. Secondly, 6FDA (191.91 g) was added into the NMP-diamine solution at a stoichiometry ratio to the diamines. Then, 665.79 g of NMP was added to adjust the solution concentration to 30 wt.%. Next, the mixture was mechanically stirred at 0°C for 24 hours to obtain a viscous polyamic acid solution. After that, acetic anhydride (220.51 g) and pyridine (85.43 g) were added to the solution to carry out a chemical imidization reaction at room temperature for 24 h. Finally, the

polyimide solution was precipitated in methanol, broken into pieces using a blender, filtered, dried at 50 ℃ in a fume hood, and at 150 ℃ in a vacuum oven for 24 h, respectively. Using this method, we could produce 255±10 g 6FDA-DAM:DAP(2:1) copolyimide in one batch with a Mw of 19.9 kDa.

2.3. Solubility Parameter Calculation

To find suitable solvents and non-solvents for formulating and precipating the polymer dope solution, a group contribution method[23] was used to calculate the solubility parameters of 6FDA-DAM:DAP(2:1) and compared with those of different solvents. Hansen's solubility parameters δ was calculated using Eq. (1):

$$\delta = \sqrt{\delta_d^2 + \delta_p^2 + \delta_h^2} \quad (1)$$

where δ_d, δ_p and δ_h were solubility parameters attributed to dispersion forces, polar interactions and hydrogen bonding, respectively. According to the Van Krevelen's group contribution method[24], the three parameters were calculated using Eq. (2):

$$\delta_d = \frac{\sum F_{di}}{V}; \delta_p = \sqrt{\frac{\sum F^2{}_{pi}}{V}}; \delta_h = \sqrt{\frac{\sum E_{hi}}{V}} \quad (2)$$

where F_{di} was the dispersion component of the molar attraction constant, F_{pi} was the polar component, E_{hi} was the contribution of hydrogen bonding forces to the cohesive energy and V was the molar volume. The solubility difference between a polymer and a solvent, $\Delta\delta_{P-S}$, was calculated using Eq. (3).

$$\delta_{P-S} = \sqrt{\left(\delta_{d,P} - \delta_{d,S}\right)^2 + \left(\delta_{p,P} - \delta_{p,S}\right)^2 + \left(\delta_{h,P} - \delta_{h,S}\right)^2} \quad (3)$$

where the subscripts, p, and s, represented polymer and solvent, respectively.

Table 1 lists the solubility parameters of 6FDA-DAM:DAP(2:1), and some commonly used solvents and non-solvents. Typically, when a polymer was soluble in

147 a solvent, the value of $\Delta\delta_{S-P}$ should be less than 5[25]. To visually observe the solubility
148 of polymer in solvents, we draw a plot by δ_v and δ_h where δ_v was the root mean square
149 of δ_d, and δ_p. As shown in Fig. 1, solvents inside the green circle indicated that their
150 $\Delta\delta_{S-P}$ were less than 5. Hence, DMAc, NMP, and THF were good solvents for 6FDA-
151 DAM:DAP(2:1), while other chemicals were non-solvents. We selected NMP as a high
152 boiling point solvent, THF as a volatile solvent, EtOH as non-solvent, and water as
153 coagulant in this work.

154 Table 1. Solubility parameters of 6FDA-DAM:DAP(2:1), solvents and non-solvents

Component	δ_d(MPa$^{1/2}$)	δ_p(MPa$^{1/2}$)	δ_h(MPa$^{1/2}$)	δ(MPa$^{1/2}$)	δ_{P-S}(MPa$^{1/2}$)
Polymer	17.94	9.81	7.73	21.9	—
NMP	18.0	12.3	7.2	23.0	2.5
DMAc	16.8	11.5	7.2	21.6	2.1
DMF	17.4	13.7	11.3	24.9	5.3
Toluene	16.8	5.7	8.0	19.5	4.3
MeOH	15.1	12.3	22.3	29.6	15.1
EtOH	15.8	8.8	19.4	26.5	11.9
Glycerol	17.4	12.1	29.3	36.2	21.7
Isopropanol	15.8	6.1	16.4	23.6	9.7
Hexane	14.9	0	0	14.9	12.9
Acetone	15.5	12.3	22.3	29.8	15.0
Water	15.6	16	42.3	47.8	35.2

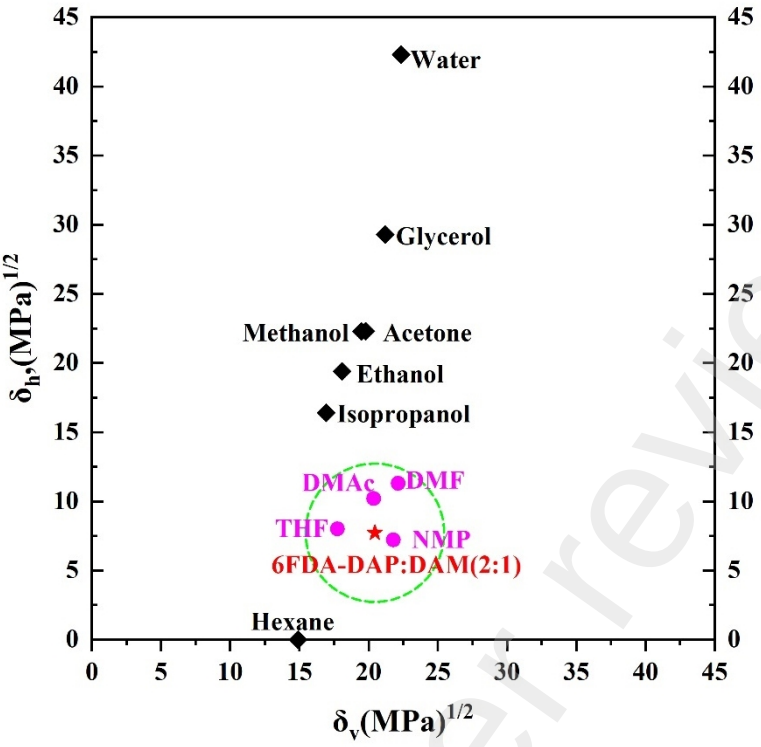

Fig. 1. Solubility parameter plot for 6FDA-DAM:DAP (2:1) and organic solvents

2.4. Cloud-point verification

A polymer/solvent/non-solvent ternary diagram with a binodal curve was constructed using a cloud point technique[26]. Points on the binodal curve, representing the initial dope composition to induce phase inversion, were determined using a titration method at 25℃. Points at the binodal curve corresponded to a polymer concentration ranging from 18 to 32 wt.%. It could be seen that water was a much stronger non-solvent than EtOH. Since the window for adjustment of EtOH was much wider than H_2O, it was used as a non-solvent additive to push the dope composition closer to the binodal curve for accelerating the phase inversion rate. The purple stars in the ternary diagram represented the dope compositions used in this work(Fig. 2).

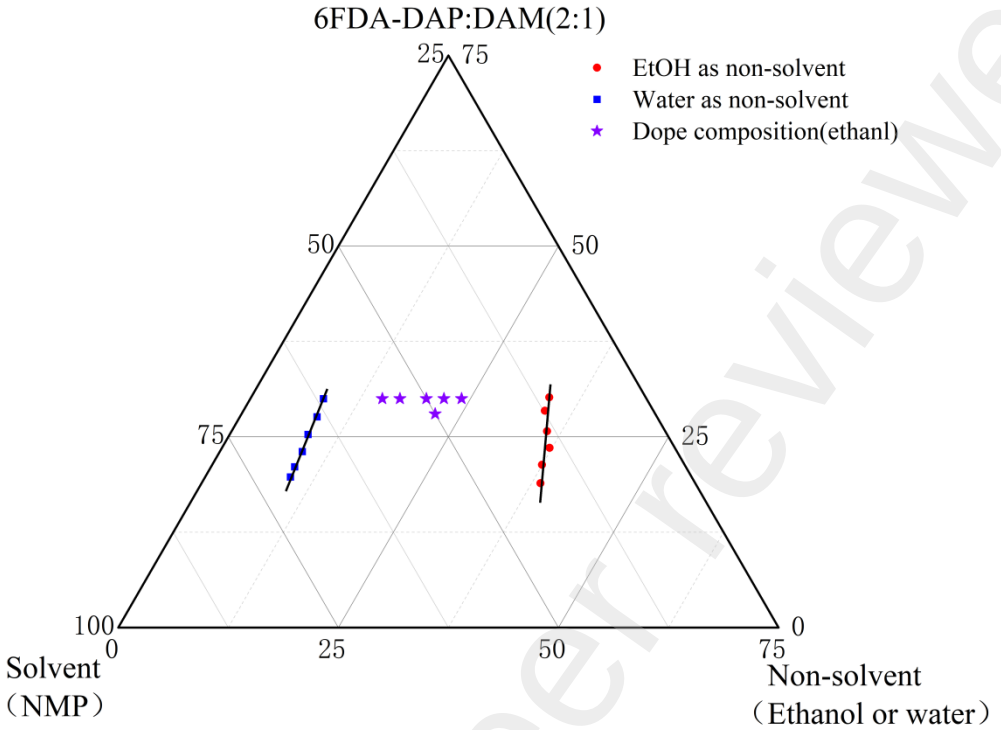

Fig. 2. A ternary phase diagram of 6FDA-DAM:DAP(2:1)/NMP/H_2O and 6FDA-DAM:DAP(2:1)/NMP/EtOH systems.

2.5. Film preparation

Dense films of 6FDA-DAM:DAP(2:1) were cast from 6FDA-DAM:DAP(2:1)-NMP solutions. The solution was filtered with a 2.0 μm PTFE filter, poured into a glass dish, vacuum dried at 60 ℃ for 24 hours, 90 ℃ for 12 hours, 120 ℃ for 12 hours, and 150 ℃ for 24 hours. Finally, the film was peeled off and used for testing gas permeabilities at 35 ℃.

2.6. Critical concentration

It was reported that there is an inflection point in the plot by polymer concentration and viscosity where the dope viscosity rapidly increased upon this concentration[27]. Defect-free hollow fiber membranes could be prepared using a polymer dope having a

concentration beyond the critical concentration where pronounced polymer chain entanglements occured. As shown in Fig. 3, the slope increased rapidly as the polymer concentration was close to 30 wt.%. Therefore, we prepared dope solutions with a polymer concentration equal or above 30 wt.% in most cases.

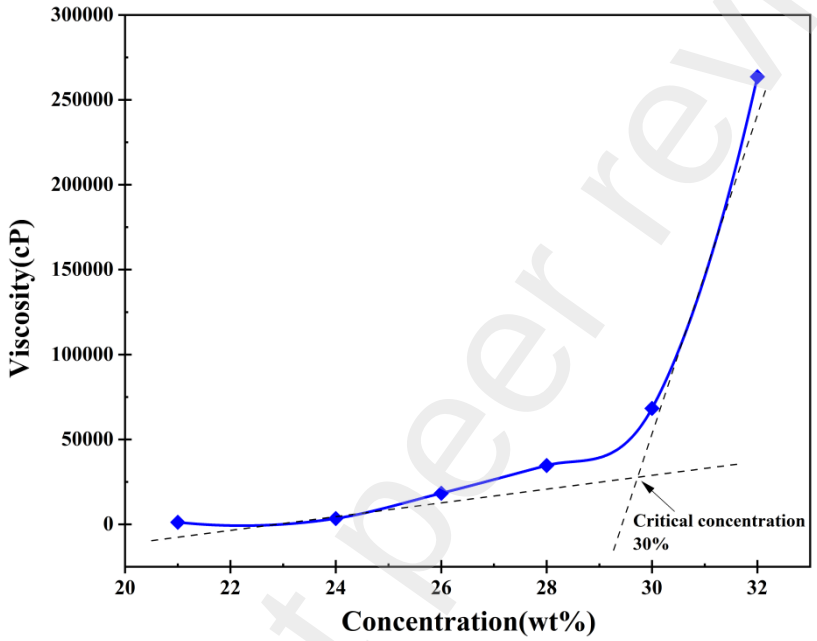

Fig. 3. The plot of dope viscosities versus polymer concentrations.

2.7 Hollow fiber spinning

Hollow fiber membrane were produced using a dry-jet/wet-spinning method using equipment illustrated in Fig. 4[28]. The dope and bore solutions were simultaneously extruded through a gear pump and a HPLC pump to a spinneret, respectively, where the outer and inner diameters were 1.4 mm and 0.6 mm, respectively. Upon exiting the spinneret, the nascent hollow fiber passed through an air gap and then into a water bath. Subsequently, the solidified hollow fiber was collected by a take-up drum. After cutting off from the drum, the fiber was soaked in water for 24 hours to eliminate remaining

solvent. After that, the fiber was soaked in a methanol bath for 30 minutes (3 times), and then in a hexane bath for 30 minutes (3 times). At last, the fiber was dried at room temperature for 1 day and then vacuum heated at 90℃ for 12 hours.

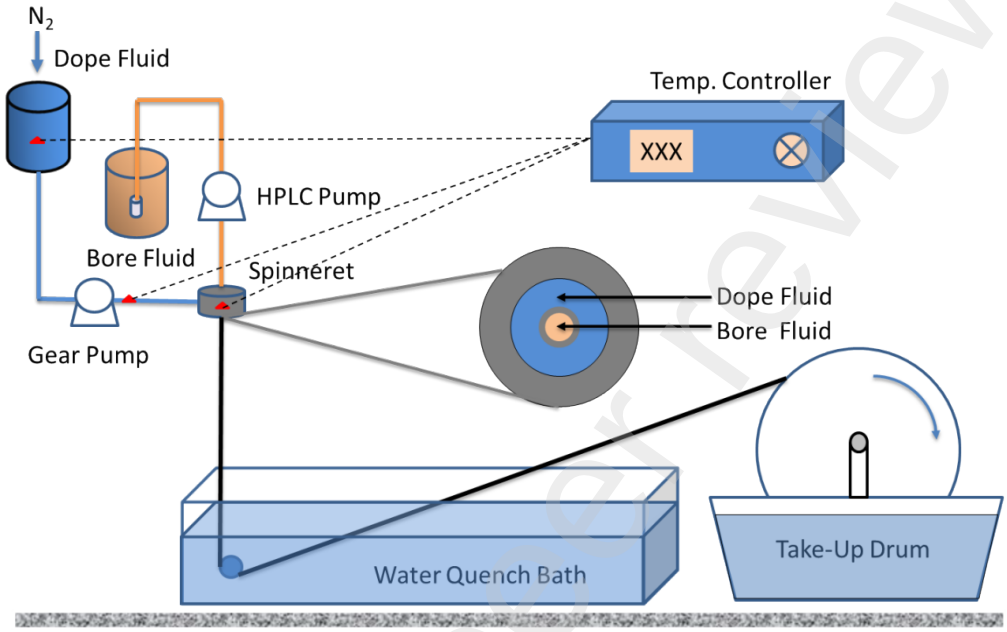

Fig. 4. A schematic diagram of the dry-jet/wet-quench spinning process for preparing asymmetric hollow fiber membrane.

2.8 Polydimethylsiloxane (PDMS) coating

Hollow fiber membrane with a ultra-thin but defective skin layer exhibit ultra-high gas permeance and maintained intrinsic selectivity after silicon rubbers coating [10]. For instance, Koros' groups spun a Matrimid hollow fiber membrane with a skin layer thickness of 25 nm. After PDMS coating, the membrane showed a CO_2 permeance of 421 GPU with a CO_2/N_2 selectivity of 31[29]. Therefore, we also adopted this PDMS coating method to enable exploitation of defective hollow fiber membranes that were highly permeable. To prepare PDMS coating solution, roughly 12 g of Sylgard 184 elastomer was pre-heated at 80 ℃ for 5-8 mins to partially crosslink the polymer.

After that, the polymer was dissolved in a cold n-hexane solution at a concentration of 3 wt.% and stored in a fridge at 2 ℃. A membrane module with 50 filaments was immersed in 3% Sylgard 184 n-hexane solution for 3 seconds, and then hanged in air for 48 hours to fully crosslink the PDMS.

2.9. Characterization

The dope viscosities were measured by an NDJ-8S rotational viscometer at 3 rpm (Yue Ping Scientific Instrument Company, Ltd. Shanghai, China). The cross-sectional morphologies of hollow fibers were investigated using a scanning electron microscope (SEM, HITACHI S-7800, Japan). To obtain a smooth surface, the sample was fractured in liquid nitrogen and then spray-coated with gold.

2.10 Determination of gas separation property

Pure gas permeabilities of H_2, N_2, O_2, CH_4, and CO_2 to dense film at 35℃ were measured using a constant volume pressure build-up method as introduced in our previous work[30]. Gas permeability (P) and ideal selectivity (α) were inferred using equation (4) and (5):

$$P = \frac{273\times10^{10}}{760}\times\frac{Vl}{AT\times\frac{76}{14.7}\times P_2}\times\frac{dp_1}{dt} \quad (4)$$

$$\alpha_{A/B} = \frac{P_A}{P_B} \quad (5)$$

where P was the permeability in Barrer [1 Barrer=1×10^{-10}cm^3(STP)·cm/(s·cm^2· cmHg)]. V (cm^3) was the volume of the downstream chamber, A(cm^2) the effective membrane area for gas transport, *l* (cm) the thickness of membrane, T (K) the testing temperature,

P_2 (psia) the upstream pressure, and dp/dt was the cumulative rate in pressure of the downstream chamber under steady state.

Gas permeance of hollow fiber membranes was measured at room temperature (20-25 ℃) with a feed pressure of 3.8 bar gauge using a lab-made equipment as introduced in our previous work [31]. Each membrane module contained 20 hollow fibers with a length of about 10 centimeters. Gas was fed on membrane shell side, while permeate was collected on the hollow fiber lumen side. A stabilization period of 30 mins was allowed before conducting gas permeation tests. Three replicated membrane modules were prepared for each test. Gas permeance ($\frac{P}{l}$) in GPU [1 GPU=1×10^{-6}cm^3 (STP)/(cm^2·s·cmHg)] was calcualted using equation (6):

$$\frac{P}{l}=\frac{273.15\times10^{6}}{T}\times\frac{Q}{A\Delta P}=\frac{273.15\times10^{6}}{T}\times\frac{Q}{\mathrm{n}\pi Dl\Delta P} \quad (6)$$

where Q (mL/s) was the flow rate of the permeate. D (cm) represented the average diameter of the hollow fiber. l (cm) was the length of the hollow fiber. ΔP represented the pressure difference between the upstream and downstream sides of the membrane. The ideal selectivity of the hollow fiber membrane was calculated using Eq. (7):

$$\alpha_{i/j}=\frac{(P/l)_i}{(P/l)_j} \quad (5)$$

where $(\frac{P}{l})_{\mathrm{i}}$ and $(\frac{P}{l})_{\mathrm{j}}$ represented the permeances of fast and slow gases.

Mixed gas transport properties of hollow fiber membranes were determined using the same gas permeance testing equipment. The ratio of permeate gas to feed gas was controlled below 1% to minimize the effect of concentration polarization[32]. The composition of permeate gases were analyzed using a gas chromatography (Model:

GC9900, JIAFEN, CN). Mixed gas permeation tests were conducted using O_2/N_2 (22:78), CO_2/N_2 (15:85), and CO_2/CH_4 (50:50) mixtures as feeds. The permeance and selectivity of the mixed gases were determined using the following equations (8) (9):

$$P_i = P \times y_i \tag{6}$$

$$\alpha^*_{i/j} = \frac{y_i / y_j}{x_i / x_j} \tag{7}$$

where P_i was permeance of component *i*, P was the total mixed gas permeance, *x* and *y* were the mole compositions of the upstream and downstream gases, respectively. y_i was the mole fraction of component *i*. $\alpha^*_{i/j}$ was the mixed gas selectivity.

3. Results and discussion

3.1. Gas transport properties of 6FDA-DAM:DAP (2:1) copolyimide

The gas transport properties of 6FDA-DAM:DAP(2:1) copolyimide dense film are summarized in Table 2. 6FDA-DAM:DAP (2:1) copolyimide combined the advantages of the high permeability of 6FDA-DAM and the high selectivity of 6FDA-DAP. That was because the bulky DAM moiety increased the inter-chain distance that favored gas transport, while the polar internal ester group of DAP strengthened the inter-molecular attraction force so that improved the molecular sieving effect. Note that, the CO_2 permeability of our 6FDA-DAM:DAP (2:1) copolyimide was significantly higher than that of commercial gas separation membrane materials including cellulose acetate, Matrimid, P84 polyimide, PSF, of which the CO_2 permeability ranged between 1 – 11 Barrer [12-14]. We expected that hollow fiber membranes fabricated from the 6FDA-DAM:DAP(2:1) copolyimide should exhibit high gas permeances with comparable selectivity. Here it is important to highlight that the O_2 permeability of the dense 6FDA-

DAM:DAP (2:1) film would be used to calculate the skin layer thickness and the ideal gas selectivities of this film would be used to determine the defectivity of hollow fiber membranes in the latter sections. A rule of thumb was that the ideal selectivity of a defect-free hollow fiber membrane should be above 90% of that of the dense film[33].

Table 2. Gas transport properties of 6FDA-DAM:DAP(2:1) dense film membrane

Copolyimide	Gas permeability (Barrer)				Ideal selectivity		
	N_2	O_2	CH_4	CO_2	O_2/N_2	CO_2/N_2	CO_2/CH_4
6FDA-DAM:DAP(2:1)	4.60	19.4	3.04	96.8	4.22	21.0	31.8
6FDA-DAM[16]	38.57	135	46.42	817	3.5	21.2	17.6
6FDA-DAP[21]	1.02	5.10	0.58	20.2	5.0	19.8	34.8

3.2. Influence of ethanol content on the formation of defect-free hollow fiber

To spin defect-free hollow fiber membranes, the starting polymer concentration was selected at 28 wt.% or 30 wt.%, one below and another above the critical concentration as shown in Fig. 3. The ratio of NMP to THF was set at 2:1 according to protocols reported elsewhere [34, 35]. Three dope compositions were tried and listed in Table 3. Temperatures of dope solution, spinneret, and coagulant bath were 50 ℃ to induce fast phase inversion rates for delivering thin skin layers. The distance of air-gap was kept at 15 cm to facilitate THF evaporation in the air-gap so that the outer-most region of the hollow fiber contains a higher polymer concentration for forming a defect-free skin layer.

Table 3. Dope compositions of 6FDA-DAM:DAP(2:1)

Component	M1(wt%)	M2(wt%)	M3(wt%)
6FDA-DAM:DAP(2:1)	28	30	28
NMP	38	33.33	33.33
THF	19	16.67	16.67
Ethanol	15	20	22

290 Table.4. Spinning parameters

Spinning parameter	Value
Dope flow rate	180 mL/h
Bore flow rate	60 mL/h
Bore fluid composition	90%/10% NMP/H_2O
Spinneret dimension	od/id 0.6/1.4 mm
Take-up rate	50 m/min
Air-gap distance	3-15 cm
Spinneret temperature	50 ℃
Quench bath temperature	50 ℃

291 The gas permeances and pure gas selectivities of hollow fiber membranes
292 fabricated from various parameters (Tables 3 and 4) are listed in Table 5. These values
293 were used to determine how ethanol content in the dope solution affected the defectivity
294 of hollow fiber membranes studied here. By comparing the O_2/N_2, CO_2/CH_4, and
295 CO_2/N_2 selectivities between hollow fiber (M1 – M3) and dense film membranes, M2
296 and M3 hollow fiber membranes were defect-free, but M1 comprised defects. Since M1
297 and M3 had the same polymer concentration, the high ethanol concentrations (≧ 20
298 wt%) in M2 and M3 dope solutions were key for forming defect-free hollow fibers.
299 Ethanol, as a non-solvent additive, drove the dope composition closer to the binodal
300 curve and accelerated phase inversion on the hollow fiber surface. The outermost region
301 of the newly formed fibers could be driven into the glassy region without traversing the
302 two-phase region, thereby reducing the formation of defects[16]. Note that, the O_2/N_2
303 (5.4) and CO_2/CH_4 (43) selectivity of hollow fibers obtained from M3 dope solution
304 were significantly higher than the intrinsic selectivities of dense copolyimide film. This
305 trend was typical of polymeric hollow fiber membranes, where better chain orientation
306 occured during the extrusion from the spinneret and take-up processes. The more

orientated chain packing condition indicated that the amount of excess free volume resulted from incompleted packing reduced. Consequently, gas selectivities of the hollow fiber membrane were higher than the dense film [15, 36]. The estimated skin layer thicknesses of M2 and M3, based on the permeance and permeability of O_2 to hollow fiber and dense film, were about 0.6 μm. However, the SEM images in Fig. 5 indicated that the dense layer regions of M2 and M3 were 340 and 357 nm, respectively. The discrepancy was caused by 1) a transition layer from the dense layer to the porous substrate that made it difficult to determine the dense layer thickness with precision based on SEM micrographs, and 2) the packing density in the polymer in the skin layer region might be higher, hence the gas permeability at the skin layer could be lower than that of the thick films. Note that, observations of higher selectivity and lower permeability for thin films with thickness of several hundred nanometers were extensively reported[37-39]. In this study, M2 and M3 showed approximately 7.8% and 31.85% higher CO_2/CH_4 selectivity than dense film.

Although defect-free hollow fiber membranes were prepared, their cross-sections were elliptical. This will consequently lead to flattened hollow fibers under high compression forces (up to 60 bar) that are typical of real-world operating conditions. Moreover, surfaces of M2 and M3 were rougher than M1 that had a regular round cross-sectional morphology but had surface defects. As the only difference between these hollow fiber types lie in the ethanol concentration in the dope solution, here this should be the reason underpinning irregular hollow fiber morphology. The cross-sections of M2 and M3 were full of sponge-like micro-voids, that indicated the phase inversion

followed nucleation growth mechanism[40]. This meant that the phase inversion rates inside M2 and M3 hollow fibers were slow. Comparing the SEM micrographs of M1 and M3 in Fig. 5c, a clear dense layer region could be only observed on M3. Therefore, we hypothesized that the irregular morphologies of M2 and M3 was caused by different phase inversion rates between the surface and inner regions of the hollow fiber membranes. During hollow fiber spinning, the outermost regions of M2 and M3 were solidified immediately, but the inner part of the hollow fiber was still in liquid state. Once the inner part started to solidified, the stress generated during solidification caused deformation of the hollow fiber membrane both on surface (higher roughness of M2 and M3) and bulk phase (elliptical cross-section)[41].

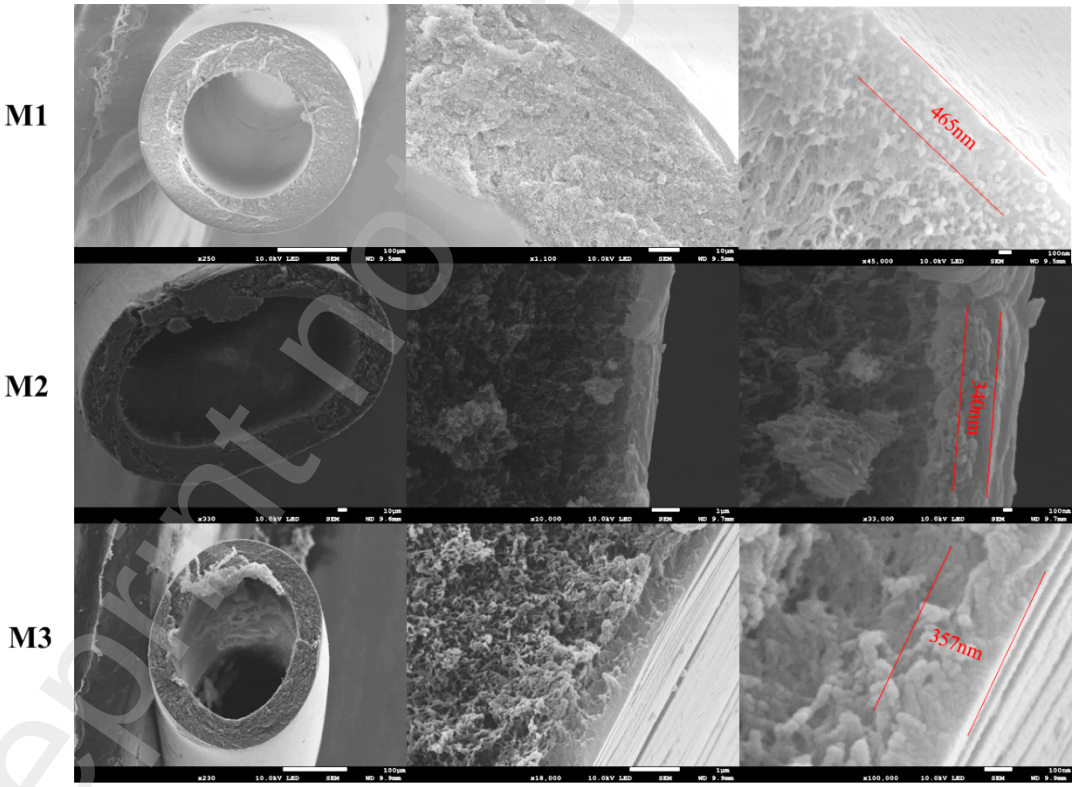

Fig. 5. The SEM images of 6FDA-DAM:DAP(2:1) hollow fiber spun from the M1, M2

and M3 dope formulation. (a) cross-section, (b) fiber wall, and (c) skin layer.

Table 5. Separation properties of hollow fibers.

Dope	Permeance (GPU)				Selectivity		
	N_2	O_2	CH_4	CO_2	O_2/N_2	CO_2/N_2	CO_2/CH_4
M1	11.4±1	35.7±5	11.1±1	127±10	3.13	11.14	11.44
M2	6.0±0.6	31.1±3	4.9±0.5	168±13	5.18	28.00	34.29
M3	4.6±0.4	24.7±2	3.7±0.4	159±11	5.37	35.43	42.97

3.4. Influence of THF content on the permeance of hollow fiber membrane

To further reduce the skin layer thickness for preventing heterogenous phase inversion rates in both the outer and inner hollow fiber regions, we reduced the THF concentrations in the dope solutions from 16.67 – 19 wt.%, to 12 – 15 wt.% (Table 6). This was to mitigate the effects of THF evaporation in the air-gap region. Other spinning parameters were the same as in Table 4. The hollow fibers were further evaluated with pure gas permeation to study ideal gas separation properties as listed in Table 7. As THF concentration in the dope solution decreased from 16.67 wt.% (M3) to 12 wt.% (M5), CO_2 permeances increased from 159 GPU to 253 GPU, while CO_2/CH_4 selectivity decreased from 43.0 to 33.3, which was still higher than the intrinsic selectivity of 31.8. As shown in Fig. 5 and Fig. 6, the dense layer thicknesses of M3 to M5 gradually decreased from 357 (M3) to 314 (M4) and 287 (M5) nm. Meanwhile, based on the O_2 permeances, the calculated skin layer thickness of M3, M4 and M5 were 600, 392 and 378 nm, respectively. Hence, the increment in gas permeance was attributed to the thinner skin layer thickness. However, this reduction in skin layer thickness came at the expense of selectivity, as the trade-off between permeance and selectivity was observed. We hypothesized that reducing THF evaporation rates by lowering THF content in dope solutions resulted in a relatively

lower polymer concentration at the surface of the nascent hollow fiber, causing loosely packed polymer chain structures in the skin layer. Moreover, the shape of M3 and M5 hollow fibers remained elliptical. Further efforts were carried out to obtain hollow fibers with regular round shape.

Table. 6. Dope compositions of 6FDA-DAM:DAP(2:1)

Component	M4(wt%)	M5(wt%)
6FDA-DAM:DAP(2:1)	30	30
NMP	33	36
THF	15	12
Ethanol	22	22

Table 7. Separation properties of M4, and M5 hollow fibers

Dope	Permeance (GPU)				Selectivity		
	N_2	O_2	CH_4	CO_2	O_2/N_2	CO_2/N_2	CO_2/CH_4
M4	7.5±0.5	42.9±5	6.3±0.3	245±18	5.72	32.7	38.9
M5	9.0±0.5	47.0±6	7.6±0.4	253±20	5.22	28.1	33.3

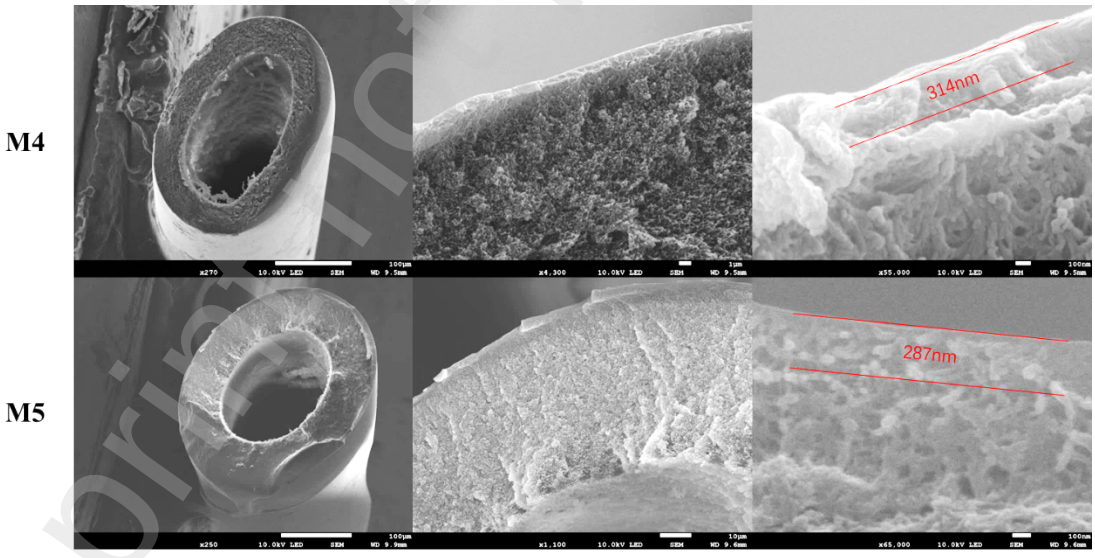

Fig. 6. SEM images of 6FDA-DAM:DAP(2:1) hollow fiber spun from the M4 and M5 dope formulation. (a) Cross-section, (b) fiber wall, and (c) skin layer.

3.5 Factors Influencing Hollow Fiber Morphology

Previous attempts indicated that defect-free hollow fiber membranes could be prepared using polymer dopes with ethanol concentration > 20 wt.% . However, this also led to the formation of oval-shaped hollow fiber membranes. During fiber spinning, we observed that the hollow fibers were round when it just exited the spinneret, and became oval upon entering the water coagulant. It was not flattened by the guiding roll in the water bath. We hypothesise that the big discrepancy between the phase inversion rates between the outermost region and the bulk phase of the hollow fiber underpinned the formation of oval-shaped hollow fibers. To validate this hypothesis, we first reduced the ethanol content in the dope composition, shifting it slightly away from the binodal curve for reducing the discrepancy in phase transition rates during the quenching process. As preparing the M6 dope solution, the ethanol content decreased to 15 wt.%. And the THF concent was reduce to 5 wt.% for achieving a thinner skin layer. For preparing the M7 dope solution, besides lowering the ethanol concentration to 15 wt.%, we added $LiNO_3$ into the dope to form a complex with NMP. We expected that once the hollow fiber (from M7 dope solution) entered the water quench, the NMP-$LiNO_3$ complex dissociated and this accelerated the phase separation rate throughout the whole hollow fiber [16]. This minimized the disparity in phase transition rates between the bulk and outer regions of the hollow fiber. Parameters outlining these two different approaches are summarized in Table 8 and the spinning parameters are the same as in Table 4. As shown in Fig. 7, hollow fibers spun from the two dope solutions had regular round cross-sectional morphologies with micro-void free structures.

393 Table 8. Optimized dope composition of 6FDA-DAM:DAP(2:1) hollow fiber spinning.

Component	M6(wt%)	M7(wt%)
6FDA-DAM:DAP(2:1)	30	30
NMP	50	43
THF	5	15
Ethanol	15	15
$LiNO_3$	-	2

394

395 Table 9. Separation properties of hollow fibers

Dope	Permeance (GPU)				Selectivity		
	N_2	O_2	CH_4	CO_2	O_2/N_2	CO_2/N_2	CO_2/CH_4
M6	27.7±2	127±7	25.3±2	713±45	4.60	25.7	28.2
M7	7.8±0.6	46.7±3	5.6±0.5	282±10	5.99	36.2	50.4
M6[a]	14.5±1	85.7±7	12.3±1	554±30	5.91	38.2	45.0

396 [a] Fibers after silicon rubber coating.

397 As listed in Table 9, the O_2 and CO_2 permeances of M6 hollow fiber reached 127
398 and 713 GPU, respectively. These gas permeances were much higher than those of M1
399 – M5 hollow fibers. The O_2/N_2 and CO_2/CH_4 selectivities of M6 were 4.60 and 28.2,
400 respectively. Although these selectivity values were more than 90% of the intrinsic
401 selectivities (dense film $\alpha_{O2/N2}$=4.22, $\alpha_{CO2/CH4}$=31.8), M6 was still defective. The effects
402 of these defects were still apparent even after PDMS coating, where the O_2/N_2 and
403 CO_2/CH_4 selectivities of PDMS coated M6 fibers reached 5.91 and 45.04, respectively,
404 while O_2 and CO_2 permeances were reduced to 85.7 and 554, respectively. Meanwhile,
405 by enabling a more homogenous phase inversion rate between the inner and outer
406 regions of a hollow fiber, the O_2 and CO_2 permeances of M7 hollow fibers reached 46.7
407 and 282 GPU, respectively. The selectivities of O_2/N_2 and CO_2/CH_4 gas pairs for M7
408 membranes were 5.99 and 50.4, respectively. Therefore, M7 was defect-free. The SEM

micrograph in Fig 7c showed that there was a clear dense layer region of 330 nm in M7 membranes. The gas permeances of M7 were lower than those of M6, possibly due to the higher viscosity of the polymer dope solution that comprised $LiNO_3$. High dope viscosity could lead to slow phase inversion rate of hollow fiber so that formed a thick skin layer[42]. Since defect-free hollow fiber membranes with regular round shape could be formed by adding $LiNO_3$ with a relatively low ethanol content（15 wt.%）, we increased $LiNO_3$ content in the dope solution to 4 and 6 wt.%. The purpose was to increase gas permeance since $LiNO_3$ was typically used as pore forming agent[43]. As shown in Table S3, higher $LiNO_3$ content in the dope solution led to the formation of hollow fibers with enhanced gas permeances at the expense of lower gas selectivities. Hence, adding 2 wt.% $LiNO_3$ into the copolyimide dope solution was ideal for forming defect-free hollow fiber membranes.

The gas selectivities of silicone-coated M6 and M7 hollow fibers were significantly higher than the intrinsic selectivity of dense film (Table 2). This could be ascribed to improved molecular orientation under high shear stress before the dope exited from the spinneret[44]. This shear stress-induced molecular orientation resulted in a higher packing density of the skin layer, leading to increments in gas selectivities of hollow fiber membranes[36, 44-47].

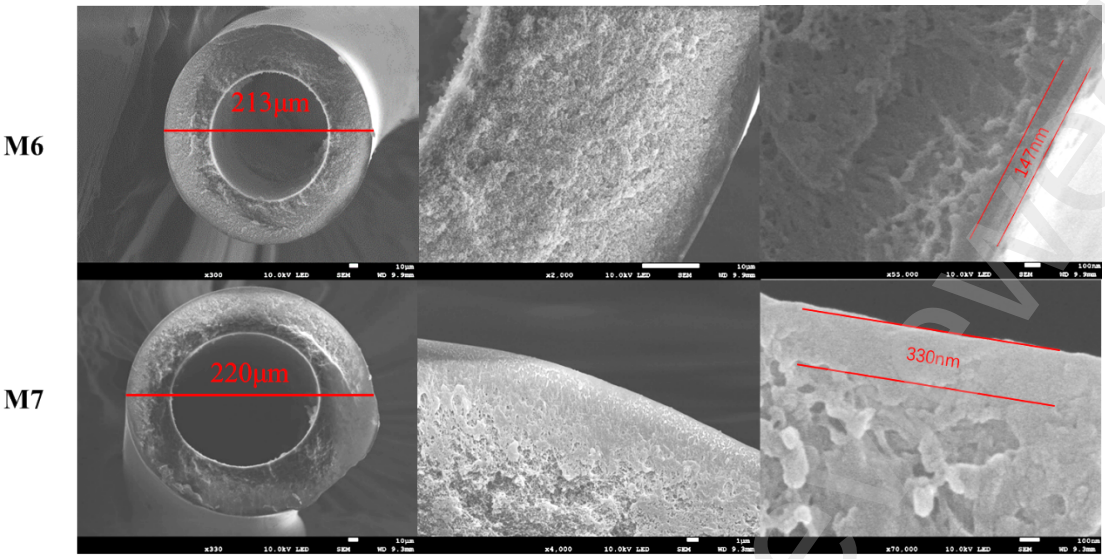

427

428 Fig. 7. SEM images of 6FDA-DAM:DAP(2:1) hollow fiber spun from the M6 and M7

429 dope formulation. (a) Cross-section, (b) fiber wall, and (c) skin layer.

430 **3.5 Influence of air-gap distance on gas separation performance**

431 Other than tailoring EtOH, THF and $LiNO_3$ content in the dope solution, here we

432 also investigated the effect of air-gap distance between the spinneret and water bath on

433 membrane defectivity (Fig .8). We observed that as the air-gap distances increased from

434 3 cm to 14 cm, CO_2 and CH_4 permeances of resultant hollow fibers were reduced by 40

435 – 99 %, while CO_2/CH_4 selectivities increased from 0.91 to 50.

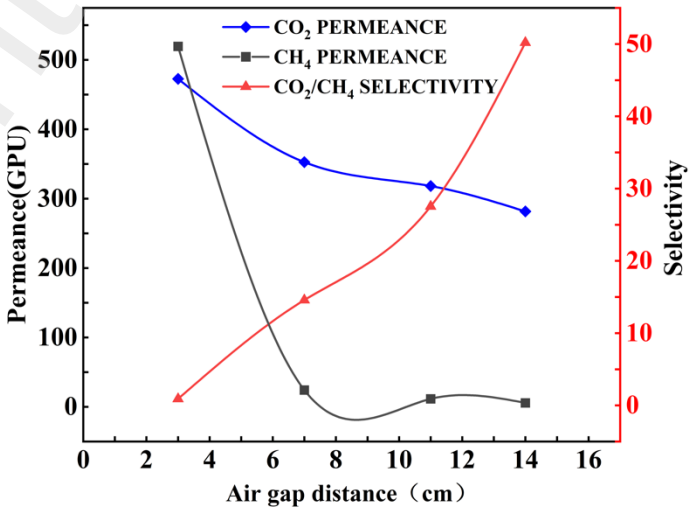

436

Fig. 8. Effects of air-gap to the CO_2/CH_4 permeance and selectivity of hollow fibers (Dope: 30% 6FDA-DAM:DAP(2:1), 43% NMP, 10% THF, 15% EtOH, 2% $LiNO_3$).

With an air-gap of 3 cm, we obtained hollow fibers with CO_2 and CH_4 permeances of 482 and 510 GPU and a CO_2/CH_4 selectivty of 0.95. Due to high viscosity, the polymer dope solution encountered high compression forces as it passed through the small orifice of the spinneret. Upon exiting the spinneret, the compression pressure would be released, and this would lead to the swelling of the dope solution. This is known as the die swell effect [48]. Although defect generation could be attributed to spinneret dimensions, dope rheology, chain relaxation, and phase inversion rates, the die swell effect was a dominant factor when the air-gap was short[44]. This caused the nascent spun hollow fiber to expand and contract suddenly, leading to deviations in thickness and minor structural imperfections. Therefore, we believe that these defective hollow fiber membranes results from the die-swell effect at air-gaps between 3 – 7 cm. This die-swell effect was mitigated by THF evaporation when the air gap > 7 cm, where the gas selectivity of resultant fibers gradually increased from 14.6 to 50.2. A defect-free hollow fiber membrane was obtained here in this work when the air-gap distance was increased to 14 cm. We also tried to fabricate hollow fibers with air gaps > 14 cm, but this resulted in hollow fiber membranes with diameters of up to 190 μm. These thin hollow fibers were easily bent and entangled during the drying process because of electrostatic attraction forces between the thin hollow fibers. Therefore, 14 cm was selected as the air-gap distance for spinning defect-free hollow fibers.

3.6 Mixed gas permeation tests and Anti-plasticization test

Pure gas anti-plasticization tests were conducted on the 6FDA-DAM:DAP (2:1) dense film using pure CO_2 and CH_4 gases (Fig. 9). The dense film was plasticized by CO_2 as the pressure exceeded 28 bar. Defect-free hollow fiber membranes (M7) were subjected to mixed gas permeation tests, using CO_2/CH_4 (1:1) mixed gas with CO_2 partial pressures ranging from 3.87 bar to 12.1. As shown in Fig. 10, the hollow fiber was plasticized by CO_2 as the pressure exceeded 8.83 bar. The CO_2 permeances of M7 hollow fibers monotonically decreased from 281 GPU to 276 GPU as the CO_2 pressure increased from 3.87 to 8.83 bar, and subsequently it increased to 278 GPU at the CO_2 pressure of 12.1 bar. On the other hand, the CO_2/CH_4 selectivity gradually decreased from 45.3 to 37.1. The relatively weak anti-plasticization behavior observed from the hollow fiber membrane could be attributed to its thin dense layer (330 nm) compared to thicker layers in dense film. Many reports claimed that thin polymer films had lower plasticization pressure than thick films[49-53]

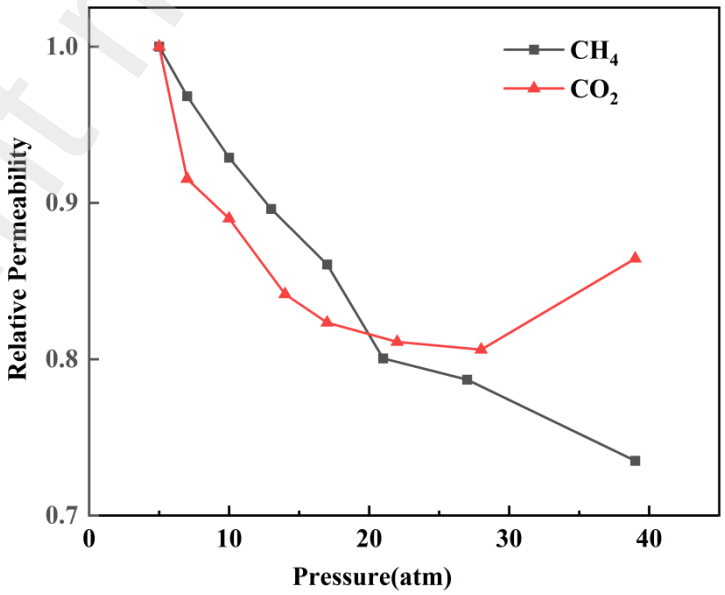

Fig. 9. The anti-CO_2 plasticization behaviors of the 6FDA-DAM:DAP (2:1) dense film

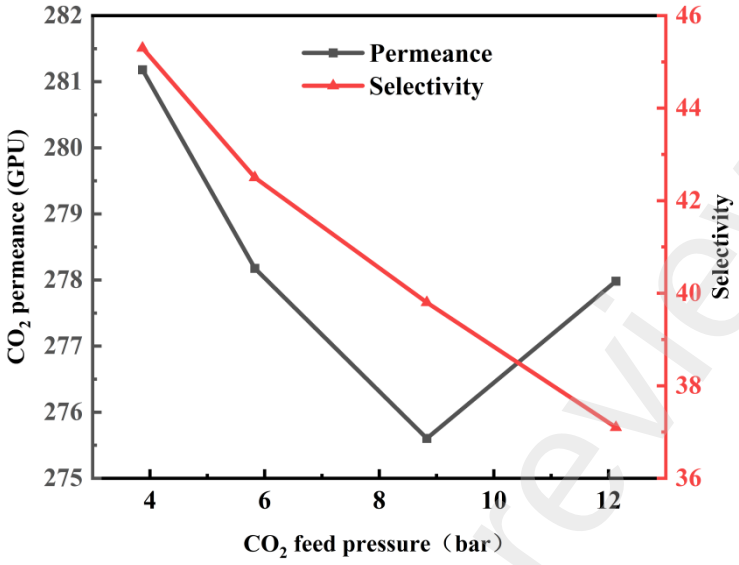

475

476 Fig. 10. The mixed gas transport properties of 6FDA-DAM:DAP (2:1) hollow fiber
477 membranes using a 50:50 CO_2/CH_4 mixed gas at a pressure up to 24.3 bar.

478 Mixed gas permeation tests were also conducted on PDMS-coated M6 and
479 without PDMS coated M7 hollow fiber membranes using CO_2/CH_4 (50:50) (at 8 bar),
480 O_2/N_2 (22:78) (at 10 bar), and CO_2/N_2 (15:85) (at 2 bar) mixed gases. Fig. 11 presents
481 a comparison of the gas separation performance of the 6FDA-DAM:DAP (2:1) hollow
482 fiber membranes with some state-of-art hollow fiber membranes in terms of O_2/N_2,
483 CO_2/CH_4, and CO_2/N_2 gas pairs. The mixed gas O_2 and CO_2 permeances of PDMS-
484 coated M6 membranes reached 73.5 and 465 GPU, respectively. Meanwhile the mixed
485 gas O_2/N_2, CO_2/CH_4 and CO_2/N_2 selectivities of PDMS-coated M6 membranes reached
486 5.4, 41.0, and 33.3, respectively. For the defect-free M7 hollow fiber, its mixed gas O_2
487 and CO_2 permeances reached 43.3 and 281 GPU, respectively, while mixed gas O_2/N_2,
488 CO_2/CH_4 and CO_2/N_2 selectivities were 5.5, 45.0, and 35.7, respectively. These
489 performances were superior to polymeric hollow fiber membranes reported elsewhere,

demonstrating their potential for commercial gas separation applications such as natural gas purification, air separation, and flue gas treatments.

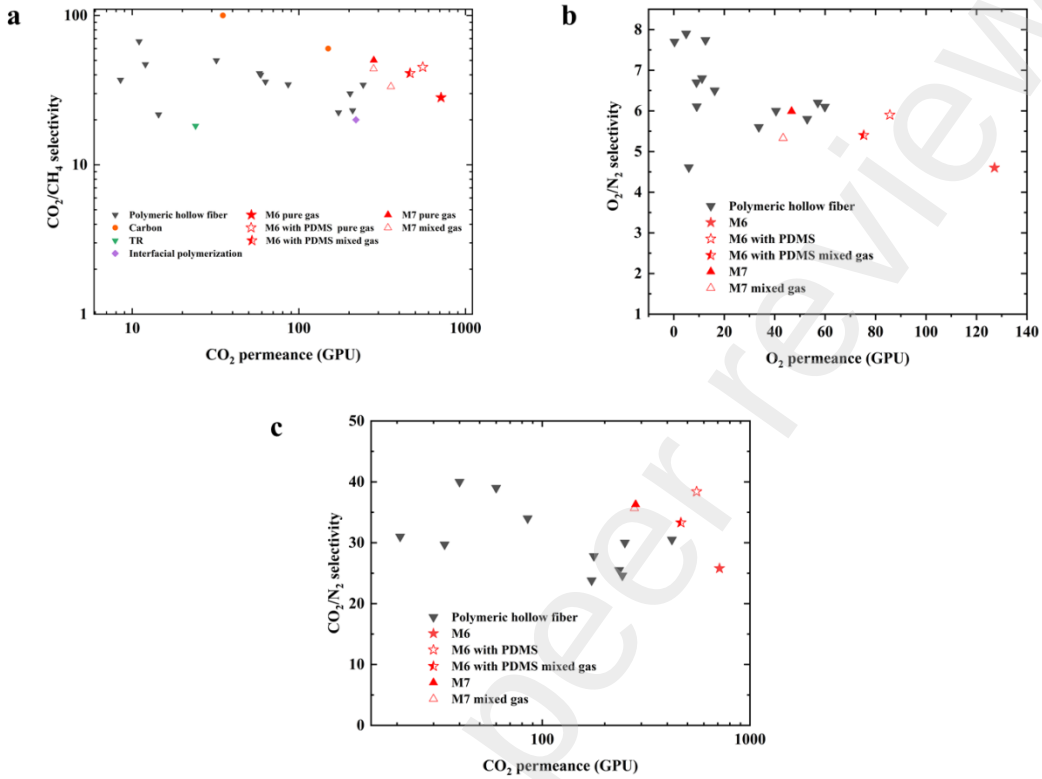

Fig. 11. Gas separation performance of 6FDA-DAM:DAP (2:1) hollow fiber membrane. (a) Literature data and present work for CO_2/CH_4 selectivity versus CO_2 permeance: Polymer[33, 34, 54-58], Carbon[59], TR[60], Interfacial polymerization[61] .(b) Literature data and present work for O_2/N_2 selectivity versus O_2 permeance [8, 33, 62-66]. (c) Literature data and present work for CO_2/N_2 selectivity versus CO_2 permeance [8, 29, 33, 65-67]. More details are listed in Table S4, S5, S6.

4. Conclusions and future works

We synthesized a novel copolyimide, 6FDA-DAM:DAP (2:1), and spun it into defect-free hollow fiber membranes using a dry-wet spinning method. Hollow fiber membranes with regular round shape was accomplished by balancing the phase

inversion rates between the surface region and bulk phase of the hollow fiber membranes. An ethanol concentration of more than 20 wt.% was found to be key for delivering defect-free hollow fibers but this also led to the formation of irregular-shaped hollow fibers that could collapse under high compression forces – conditions typical of real-world operation. To overcome this limitation without generating defects, we lowered the ethanol concentration to 15 wt.%, added $LiNO_3$ and adopted a higher air-gap. Notably, both PDMS-coated defective hollow fiber membranes and defect-free hollow fiber membrane exhibited much higher gas selectivity than the dense film. We attributed this to the better orientation of polymer chains of the hollow fiber membrane induced by a higher extrusion rate of the spinneret, hence yielding hollow fiber membranes with desired separation properties.

Future endeavors could explore methods to increase the polymer molecular weight, aiming to fabricate thinner, defect-free skin layers. Additionally, the copolyimide could be further modified with thermal treatment to yield high performance thermally rearranged polymers to deliver improved gas separation performances and anti-plasticization behaviors.

Acknowledgements:

LP acknowledges funding from China Petroleum and Chemical Corporation (Project code: 222126) for this work.

5. Reference

[1] S.S. Hosseini, T.S. Chung, Carbon membranes from blends of PBI and polyimides for N2/CH4 and CO2/CH4 separation and hydrogen purification, J. Membr. Sci., 328 (2009) 174-

525 185.

526 [2] M. Ashraf Chaudhry, R. Raza, S.A. Hayat, Renewable energy technologies in Pakistan:
527 Prospects and challenges, Renewable and Sustainable Energy Reviews, 13 (2009) 1657-1662.

528 [3] R.P. Lively, R.R. Chance, B.T. Kelley, H.W. Deckman, J.H. Drese, C.W. Jones, W.J. Koros,
529 Hollow Fiber Adsorbents for CO2 Removal from Flue Gas, Industrial & Engineering Chemistry
530 Research, 48 (2009) 7314-7324.

531 [4] A. Fernández-Barquín, C. Casado-Coterillo, S. Valencia, A. Irabien, Mixed Matrix Membranes
532 for O2/N2 Separation: The Influence of Temperature, in: Membranes, 2016.

533 [5] R.W. Baker, Future Directions of Membrane Gas Separation Technology, Industrial &
534 Engineering Chemistry Research, 41 (2002) 1393-1411.

535 [6] W.H. Lee, J.G. Seong, X. Hu, Y.M. Lee, Recent progress in microporous polymers from
536 thermally rearranged polymers and polymers of intrinsic microporosity for membrane gas
537 separation: Pushing performance limits and revisiting trade-off lines, Journal of Polymer Science,
538 58 (2020) 2450-2466.

539 [7] P.M. Budd, N.B. McKeown, Highly permeable polymers for gas separation membranes,
540 Polymer Chemistry, 1 (2010).

541 [8] D.T. Clausi, W.J. Koros, Formation of defect-free polyimide hollow fiber membranes for gas
542 separations, J. Membr. Sci., 167 (2000) 79-89.

543 [9] G. George, N. Bhoria, S. AlHallaq, A. Abdala, V. Mittal, Polymer membranes for acid gas
544 removal from natural gas, Sep. Purif. Technol., 158 (2016) 333-356.

545 [10] D.W. Wallace, J. Williams, C. Staudt-Bickel, W.J. Koros, Characterization of crosslinked
546 hollow fiber membranes, Polymer, 47 (2006) 1207-1216.

547 [11] C. Ma, C. Zhang, Y. Labreche, S. Fu, L. Liu, W.J. Koros, Thin-skinned intrinsically defect-
548 free asymmetric mono-esterified hollow fiber precursors for crosslinkable polyimide gas
549 separation membranes, J. Membr. Sci., 493 (2015) 252-262.
550 [12] N. Widiastuti, T. Gunawan, H. Fansuri, W.N.W. Salleh, A.F. Ismail, N. Sazali, P84/ZCC
551 Hollow Fiber Mixed Matrix Membrane with PDMS Coating to Enhance Air Separation Performance,
552 Membranes (Basel), 10 (2020).
553 [13] A.F. Ismail, P.Y. Lai, Effects of phase inversion and rheological factors on formation of
554 defect-free and ultrathin-skinned asymmetric polysulfone membranes for gas separation, Sep.
555 Purif. Technol., 33 (2003) 127-143.
556 [14] V. Vatanpour, M.E. Pasaoglu, H. Barzegar, O.O. Teber, R. Kaya, M. Bastug, A. Khataee, I.
557 Koyuncu, Cellulose acetate in fabrication of polymeric membranes: A review, Chemosphere, 295
558 (2022) 133914.
559 [15] M. Niwa, H. Kawakami, S. Nagaoka, T. Kanamori, T. Shinbo, Fabrication of an asymmetric
560 polyimide hollow fiber with a defect-free surface skin layer, J. Membr. Sci., 171 (2000) 253-
561 261.
562 [16] L. Xu, C. Zhang, M. Rungta, W. Qiu, J. Liu, W.J. Koros, Formation of defect-free 6FDA-DAM
563 asymmetric hollow fiber membranes for gas separations, J. Membr. Sci., 459 (2014) 223-232.
564 [17] J. Ren, R. Wang, T.-S. Chung, D.F. Li, Y. Liu, The effects of chemical modifications on
565 morphology and performance of 6FDA-ODA/NDA hollow fiber membranes for CO2/CH4
566 separation, J. Membr. Sci., 222 (2003) 133-147.
567 [18] T.-S. Chung, E.R. Kafchinski, R. Vora, Development of a defect-free 6FDA-durene
568 asymmetric hollow fiber and its composite hollow fibers, J. Membr. Sci., 88 (1994) 21-36.

569 [19] M.R. Kosuri, W.J. Koros, Defect-free asymmetric hollow fiber membranes from Torlon®, a
570 polyamide–imide polymer, for high-pressure CO2 separations, J. Membr. Sci., 320 (2008) 65-
571 72.
572 [20] P. Du, Z. Wang, T. Zhang, C.H. Lau, S. Liu, P. Li, Crosslinked thermally rearranged
573 polybenzoxazole derived from phenolphthalein-based polyimide for gas separation, J. Membr.
574 Sci., 662 (2022).
575 [21] F. Wang, Y. Liu, P. Du, Z. Wang, G. Tang, P. Qin, P. Li, Sub-Tg cross-linked thermally
576 rearranged polybenzoxazole derived from phenolphthalein diamine for natural gas purification, J.
577 Membr. Sci., 687 (2023) 122033.
578 [22] R.P. Lively, M.E. Dose, L. Xu, J.T. Vaughn, J.R. Johnson, J.A. Thompson, K. Zhang, M.E.
579 Lydon, J.-S. Lee, L. Liu, Z. Hu, O. Karvan, M.J. Realff, W.J. Koros, A high-flux polyimide hollow
580 fiber membrane to minimize footprint and energy penalty for CO2 recovery from flue gas, J.
581 Membr. Sci., 423-424 (2012) 302-313.
582 [23] C. M. Hansen, Hansen Solubility Parameters: A User's Handbook, CRC Press, 2007.
583 [24] D.W. Van Krevelen, K. Te Nijenhuis, Volumetric Properties, in: Properties of Polymers,
584 2009, pp. 71-108.
585 [25] K.Y. Wang, M. Weber, T.S. Chung, Polybenzimidazoles (PBIs) and state-of-the-art PBI hollow
586 fiber membranes for water, organic solvent and gas separations: a review, Journal of Materials
587 Chemistry A, 10 (2022) 8687-8718.
588 [26] R.M. Boom, T. van den Boomgaard, J.W.A. van den Berg, C.A. Smolders, Linearized
589 cloudpoint curve correlation for ternary systems consisting of one polymer, one solvent and one
590 non-solvent, Polymer, 34 (1993) 2348-2356.

591 [27] J. Ren, T.-S. Chung, D. Li, R. Wang, Y. Liu, Development of asymmetric 6FDA-2,6 DAT hollow
592 fiber membranes for CO2/CH4 separation: 1. The influence of dope composition and rheology
593 on membrane morphology and separation performance, J. Membr. Sci., 207 (2002) 227-240.
594 [28] Y. Li, B. Cao, P. Li, Fabrication of PMDA-ODA hollow fibers with regular cross-section
595 morphologies and study on the formation mechanism, J. Membr. Sci., 544 (2017) 1-11.
596 [29] L. Liu, E.S. Sanders, S.S. Kulkarni, D.J. Hasse, W.J. Koros, Sub-ambient temperature flue
597 gas carbon dioxide capture via Matrimid® hollow fiber membranes, J. Membr. Sci., 465 (2014)
598 49-55.
599 [30] C. Zhang, P. Li, B. Cao, Effects of the side groups of the spirobichroman-based diamines
600 on the chain packing and gas separation properties of the polyimides, J. Membr. Sci., 530 (2017)
601 176-184.
602 [31] W. Han, C. Zhang, M. Zhao, F. Yang, Y. Yang, Y. Weng, Post-modification of PIM-1 and
603 simultaneously in situ synthesis of porous polymer networks into PIM-1 matrix to enhance CO2
604 separation performance, J. Membr. Sci., 636 (2021).
605 [32] J.H. Shin, H.J. Yu, H. An, A.S. Lee, S.S. Hwang, S.Y. Lee, J.S. Lee, Rigid double-stranded
606 siloxane-induced high-flux carbon molecular sieve hollow fiber membranes for CO2/CH4
607 separation, J. Membr. Sci., 570-571 (2019) 504-512.
608 [33] W.F. Yong, F.Y. Li, Y.C. Xiao, T.S. Chung, Y.W. Tong, High performance PIM-1/Matrimid
609 hollow fiber membranes for CO2/CH4, O2/N2 and CO2/N2 separation, J. Membr. Sci., 443
610 (2013) 156-169.
611 [34] G. Dong, H. Li, V. Chen, Factors affect defect-free Matrimid® hollow fiber gas separation
612 performance in natural gas purification, J. Membr. Sci., 353 (2010) 17-27.

613 [35] H.S. Lau, W.F. Yong, Recent progress and prospects of polymeric hollow fiber membranes
614 for gas application, water vapor separation and particulate matter removal, Journal of Materials
615 Chemistry A, 9 (2021) 26454-26497.
616 [36] M. Niwa, Surface orientation effect of asymmetric polyimide hollow fibers on their gas
617 transport properties, J. Membr. Sci., 230 (2004) 141-148.
618 [37] J.N. Barsema, G.C. Kapantaidakis, N.F.A. van der Vegt, G.H. Koops, M. Wessling,
619 Preparation and characterization of highly selective dense and hollow fiber asymmetric
620 membranes based on BTDA-TDI/MDI co-polyimide, J. Membr. Sci., 216 (2003) 195-205.
621 [38] P.H. Pfromm, W.J. Koros, Accelerated physical ageing of thin glassy polymer films: evidence
622 from gas transport measurements, Polymer, 36 (1995) 2379-2387.
623 [39] I. Pinnau, M.W. Hellums, W.J. Koros, Gas transport through homogeneous and asymmetric
624 polyestercarbonate membranes, Polymer, 32 (1991) 2612-2617.
625 [40] A.F. Ismail, L.P. Yean, Review on the development of defect-free and ultrathin-skinned
626 asymmetric membranes for gas separation through manipulation of phase inversion and
627 rheological factors, J. Appl. Polym. Sci., 88 (2003) 442-451.
628 [41] M.L. Jue, V. Breedveld, R.P. Lively, Defect-free PIM-1 hollow fiber membranes, J. Membr.
629 Sci., 530 (2017) 33-41.
630 [42] T.S. Chung, S.K. Teoh, X. Hu, Formation of ultrathin high-performance polyethersulfone
631 hollow-fiber membranes, J. Membr. Sci., 133 (1997) 161-175.
632 [43] X.Y. Chen, S. Kaliaguine, D. Rodrigue, A Comparison between Several Commercial Polymer
633 Hollow Fiber Membranes for Gas Separation, Journal of Membrane and Separation Technology,
634 6 (2017) 1-15.

635 [44] J.-J. Qin, R. Wang, T.-S. Chung, Investigation of shear stress effect within a spinneret on
636 flux, separation and thermomechanical properties of hollow fiber ultrafiltration membranes, J.
637 Membr. Sci., 175 (2000) 197-213.
638 [45] H.K. M Niwa , S Nagaoka, T Kanamori, T Shinbo, Fabrication of an asymmetric polyimide
639 hollow fiber with a defect-free surface skin layer, Fabrication of an asymmetric polyimide hollow
640 fiber with a defect-free surface skin layer, 171 (2000) 253-261.
641 [46] T.-S. Chung, W.-H. Lin, R.H. Vora, The effect of shear rates on gas separation performance
642 of 6FDA-durene polyimide hollow fibers, J. Membr. Sci., 167 (2000) 55-66.
643 [47] A.F. Ismail, I.R. Dunkin, S.L. Gallivan, S.J. Shilton, Production of super selective polysulfone
644 hollow fiber membranes for gas separation, Polymer, 40 (1999) 6499-6506.
645 [48] N. Peng, T.S. Chung, The effects of spinneret dimension and hollow fiber dimension on gas
646 separation performance of ultra-thin defect-free Torlon® hollow fiber membranes, J. Membr. Sci.,
647 310 (2008) 455-465.
648 [49] G. Dong, H. Li, V. Chen, Plasticization mechanisms and effects of thermal annealing of
649 Matrimid hollow fiber membranes for CO2 removal, J. Membr. Sci., 369 (2011) 206-220.
650 [50] C.-C. Chen, W. Qiu, S.J. Miller, W.J. Koros, Plasticization-resistant hollow fiber membranes
651 for CO2/CH4 separation based on a thermally crosslinkable polyimide, J. Membr. Sci., 382
652 (2011) 212-221.
653 [51] C.A. Scholes, G.Q. Chen, G.W. Stevens, S.E. Kentish, Plasticization of ultra-thin polysulfone
654 membranes by carbon dioxide, J. Membr. Sci., 346 (2010) 208-214.
655 [52] N.R. Horn, D.R. Paul, Carbon dioxide plasticization and conditioning effects in thick vs. thin
656 glassy polymer films, Polymer, 52 (2011) 1619-1627.

657 [53] M. Wessling, M. Lidon Lopez, H. Strathmann, Accelerated plasticization of thin-film
658 composite membranes used in gas separation, Sep. Purif. Technol., 24 (2001) 223-233.
659 [54] C. Cao, R. Wang, T.S. Chung, Y. Liu, Formation of high-performance 6FDA-2,6-DAT
660 asymmetric composite hollow fiber membranes for CO2/CH4 separation, J. Membr. Sci., 209
661 (2002) 309-319.
662 [55] N.L. Le, Y. Wang, T.-S. Chung, Synthesis, cross-linking modifications of 6FDA-NDA/DABA
663 polyimide membranes for ethanol dehydration via pervaporation, J. Membr. Sci., 415-416 (2012)
664 109-121.
665 [56] I.C. Omole, R.T. Adams, S.J. Miller, W.J. Koros, Effects of CO2 on a High Performance
666 Hollow-Fiber Membrane for Natural Gas Purification, Industrial & Engineering Chemistry
667 Research, 49 (2010) 4887-4896.
668 [57] Y. Li, T.-S. Chung, Y. Xiao, Superior gas separation performance of dual-layer hollow fiber
669 membranes with an ultrathin dense-selective layer, J. Membr. Sci., 325 (2008) 23-27.
670 [58] Y.H. Cao, K. Zhang, O. Sanyal, W.J. Koros, Carbon Molecular Sieve Membrane Preparation
671 by Economical Coating and Pyrolysis of Porous Polymer Hollow Fibers (vol 58, pg 12149, 2019),
672 Angewandte Chemie-International Edition, 59 (2020) 21812-21812.
673 [59] N. Bhuwania, Y. Labreche, C.S.K. Achoundong, J. Baltazar, S.K. Burgess, S. Karwa, L. Xu,
674 C.L. Henderson, P.J. Williams, W.J. Koros, Engineering substructure morphology of asymmetric
675 carbon molecular sieve hollow fiber membranes, Carbon, 76 (2014) 417-434.
676 [60] L. Ye, X. Jie, L. Wang, G. Xu, Y. Sun, G. Kang, Y. Cao, Preparation and gas separation
677 performance of thermally rearranged poly(benzoxazole-co-amide) (TR-PBOA) hollow fiber
678 membranes deriving from polyamides, Sep. Purif. Technol., 257 (2021) 117870.

679 [61] X. Xu, J. Dong, X. Xiao, X. Zhao, Q. Zhang, Constructing Thin and Cross-Linked Polyimide
680 Membranes by Interfacial Reaction for Efficient CO2 Separation, ACS Sustainable Chemistry &
681 Engineering, 9 (2021) 5546-5556.
682 [62] L. Jiang, T.-S. Chung, D.F. Li, C. Cao, S. Kulprathipanja, Fabrication of
683 Matrimid/polyethersulfone dual-layer hollow fiber membranes for gas separation, J. Membr. Sci.,
684 240 (2004) 91-103.
685 [63] T. Visser, N. Masetto, M. Wessling, Materials dependence of mixed gas plasticization
686 behavior in asymmetric membranes, J. Membr. Sci., 306 (2007) 16-28.
687 [64] M.R. Kosuri, W.J. Koros, Defect-free asymmetric hollow fiber membranes from Torlon®, a
688 polyamide–imide polymer, for high-pressure CO2 separations, J. Membr. Sci., 320 (2008) 65-
689 72.
690 [65] W.F. Yong, T.-S. Chung, M. Weber, C. Maletzko, New polyethersulfone (PESU) hollow fiber
691 membranes for CO2 capture, J. Membr. Sci., 552 (2018) 305-314.
692 [66] X. Ding, Y. Cao, H. Zhao, L. Wang, Interfacial morphology between the two layers of the
693 dual-layer asymmetric hollow fiber membranes fabricated by co-extrusion and dry-jet wet-
694 spinning phase-inversion techniques, J. Membr. Sci., 444 (2013) 482-492.
695 [67] L. Hao, J. Zuo, T.S. Chung, Formation of Defect-Free Polyetherimide/PIM-1 Hollow Fiber
696 Membranes for Gas Separation, AlChE J., 60 (2014) 3848-3858.
697